View metadata, citation and similar papers at core.ac.uk

brought to you by CORE

provided by Texas A&M Repository

LANDSCAPE SCALE IMPACTS OF SEA LEVEL RISE AND ELEVATION CHANGES ALONG THE MATAGORDA FAULT IN MATAGORDA, TEXAS

A Thesis

by

MARIE DENISE CLINE

Submitted to the Office of Graduate Studies of
Texas A&M University
in partial fulfillment of the requirements for the degree of

MASTER OF SCIENCE

August 2012

Major Subject: Rangeland Ecology and Management

Landscape Scale Impacts of Sea Level Rise and Elevation Changes

Along the Matagorda Fault in Matagorda, Texas

Copyright 2012 Marie Denise Cline

LANDSCAPE SCALE IMPACTS OF SEA LEVEL RISE AND ELEVATION CHANGES ALONG THE MATAGORDA FAULT IN MATAGORDA, TEXAS

A Thesis

by

MARIE DENISE CLINE

Submitted to the Office of Graduate Studies of
Texas A&M University
in partial fulfillment of the requirements for the degree of

MASTER OF SCIENCE

Approved by:

Chair of Committee,	Rusty Feagin
Committee Members,	Sorin Popescu
	William Grant
Head of Department,	David Baltensperger

August 2012

Major Subject: Rangeland Ecology and Management

ABSTRACT

Landscape Scale Impacts of Sea Level Rise and Elevation

Changes Along the Matagorda Fault in Matagorda, Texas. (August 2012)

Marie Denise Cline, B.S., Texas A&M University

Chair of Advisory Committee: Dr. Rusty Feagin

Movement of growth faults, a type of normal fault which is formed during sedimentation and is characterized by having greater vertical thickness on the downthrown fault side, on barrier islands contributes to wetland losses. The opening objective of this study was to quantify land cover change within a Matagorda, Texas wetland that results from sea level rise and elevation change over time due to coastal faulting. The closing objective of this study was to simulate land cover conversion as a function of relative sea level rise (RSLR) within the wetland and to compare and contrast the impact of specific rates of both fault-induced elevation change and predicted International Panel on Climate Change (IPCC) sea level rise projections.

To accomplish these objectives a time series of aerial images was classified using automated unsupervised classification and hand digitization. After classification, total wetland losses on both the upthrown and downthrown sides of the fault were evaluated as a function of spatial distance from the fault plane. This classified product was draped over a digital elevation model (DEM) layer to evaluate elevations of land cover classes and model potential future outcomes based on RSLR.

Classification results show that while wetland loss occurred on both sides of the fault, losses were far more extensive on the downthrown side. It was concluded that this vertical fault movement impacts wetland losses, especially on the downthrown side. Modeling results show that rapid water level rise can force wetland land cover class conversion regardless of whether this relative rise is caused by vertical fault displacement or eustatic sea level rise, resulting in the destruction of vital wetland areas. Current recorded conditions of sea level rise along the Texas Gulf Coast leave a grim outlook for regions similar to this study area.

DEDICATION

To those who are concerned about the future of our coast

ACKNOWLEDGEMENTS

I would like to thank my committee chair, Dr. Feagin, and my committee members, Dr. Popescu and Dr. Grant, for their guidance and support throughout the course of this research.

Thanks also to my colleagues and the department faculty and staff for their support and making my time at Texas A&M University a great experience.

Finally, thanks to my family for their encouragement and my friends for their love and support. Thanks for being my rock.

NOMENCLATURE

RSLR	Relative Sea Level Rise
IPCC	International Panel on Climate Change
GIS	Geographical Information System
AOI	Area of Interest
GCP	Ground Control Point
DEM	Digital Elevation Model
LiDAR	Light Detection and Ranging
NAVD88	North American Vertical Datum of 1988
ISODATA	Iterative Self-Organizing Data Analysis Technique
TNRIS	Texas Natural Resource Information System
SPOT	Système Pour l'Observation de la Terre

TABLE OF CONTENTS

Page

ABSTRACT iii

DEDICATION v

ACKNOWLEDGEMENTS vi

NOMENCLATURE vii

TABLE OF CONTENTS viii

LIST OF FIGURES x

LIST OF TABLES xii

1. INTRODUCTION 1

2. FAULT-INDUCED WETLAND LOSS AT MATAGORDA, TEXAS, USA: LAND COVER CHANGES FROM 1943 TO 2008 3

    2.1 Introduction 3
    2.2 Methods 5
        2.2.1 Study Area 5
        2.2.2 Image Classification and Analysis 7
        2.2.3 Digitization 9
        2.2.4 Data Analysis 9
        2.2.5 Accuracy Assessment 11
    2.3 Results 12
        2.3.1 Full Extent 12
        2.3.2 Upthrown Extent 12
        2.3.3 Downthrown Extent 14
        2.3.4 Change Detection Analysis 14
        2.3.5 Fault Strips 16
    2.4 Discussion 17

3. MODELING RELATIVE SEA LEVEL RISE IN COASTAL WETLANDS: GROWTH FAULT MOVEMENT AS A PROXY FOR UNDERSTANDING THE IMPACT OF CLIMATE CHANGE 19

3.1 Introduction 19
3.2 Methods 22
3.2.1 Study Area 22
3.2.2 Imagery and Classification of Vegetation Zones 22
3.2.3 Elevation Ranges of the Zones 24
3.2.4 Accretion 25
3.2.5 Fault Strips 25
3.2.6 RSLR Simulation 27
3.3 Results 28
3.4 Discussion 33

4. SUMMARY AND CONCLUSIONS 37

REFERENCES 39

VITA 46

LIST OF FIGURES

FIGURE		Page
1	a) Geographic location of the study site on the Texas coast. b) SPOT imagery of the study site in relation to surrounding features in 1995. Delineation of the study area is represented by the solid line and delineation of the surface fault expression is represented by the dashed line.	6
2	Classified images of the study area located in Matagorda, Texas.	10
3	a) Line graph displaying transition of land area loss and water area gain from 1943 to 2008 in ha. b) Bar graph displaying transition of specific land cover classes in 1943, 1978, 1996, and 2008 in ha.	12
4	Line graphs displaying transition (in ha) from 1943 to 2008 of a) upthrown land area loss and upthrown water area gain; and b) downthrown land area loss and downthrown water area gain. Bar graphs displaying transition of specific land cover classes (in ha) in 1943, 1978, 1996, and 2008 c) within the upthrown extent; and d) within the downthrown extent.	13
5	Display of from-to change analysis (1943 to 2008, in ha) for (a) water area, (b) low marsh area, (c) salt flat area, and (d) high marsh area.	15
6	Change of area (ha) between 1943 and 2008 at designated distances from the fault in 20 m strips, with 0 m representing the fault trace at the surface. Positive and negative values on the x-axis represent increasing distances from the fault trace on the downthrown, and upthrown sides, respectively.	16
7	(a) Geographic location of the study site on the Texas coast. (b) SPOT imagery of the study site in relation to surrounding features in 1995. Delineation of the study area is represented by the solid line and delineation of the surface fault expression is represented by the dashed line. (c) fault strip locations in relation to the study area and the surface expression of the fault. (d) fault strip numbers 1-7, as described in the text and Table 1.	23
8	A frequency distribution of each vegetation zone with respect to elevation…	24

FIGURE Page

9 (a) Vegetation zone distribution in 2008, as based on the classified LIDAR data (b) Predicted vegetation zone distribution in 2050. 29

10 Predicted vegetation zone distribution, assuming the following conditions implemented across the entire landscape: (a) fault strip 1 rate in 2050, (b) fault strip 1 rate in 2100, (c) fault strip 2 rate in 2050, (d) fault strip rate 2 in 2100, (e) fault strip 3 rate in 2050, (f) fault strip 3 rate in 2100, (g) fault strip 4 rate in 2050, (h) fault strip 4 rate in 2100, (i) fault strip 5 rate in 2050, (j) fault strip 5 rate in 2100, (k) fault strip 6 rate in 2050, (l) fault strip 6 rate in 2100, (m) fault strip 7 rate in 2050, and (n) fault strip 7 rate in 2100. North is to the top of each image. Relative scale and color legend is the same as Figure 3. 31

11 Predicted vegetation zone distribution assuming the: (a) IPCC low scenario (0.18 m) in 2050, (b) IPCC low SLR scenario (0.18 m) in 2100, (c) IPCC mid SLR scenario (0.39) in 2050, (d) IPCC mid SLR scenario (0.39) in 2100, (e) IPCC high SLR scenario (0.59) in 2050, (f) IPCC high SLR scenario (0.59) in 2100, (g) an extreme SLR scenario (1.4 m) after in 2050, and (h) an extreme SLR scenario (1.4 m) in 2100. Map orientation, scale, and legend features are consistent to that of Figure 4. North is to the top of each image. Relative scale and color legend is the same as Figure 3. 32

12 Percent conversion of tidal wetland (gains exceed 100%, losses are less than 100%) into open water, as a function of RSLR for all scenarios, for the years (a) 2050, and (b) 2100. Numerical labeled data points refer to fault strip rates of vertical change (see Table 1 and Figure 4). For alpha labeled data points: L is IPCC low scenario, M is IPCC mid scenario, H is IPCC high scenario, and E is the more extreme Rahmstorf (2007) scenario. 34

LIST OF TABLES

TABLE Page

1 Fault strip reference numbers with location proximal to fault location and vertical fault strip movement rate..... 26

1. INTRODUCTION

Wetlands perform a variety of essential services for society and are an essential component of a balanced coastal ecosystem. Both climate change and relative sea level rise (RSLR) threaten the stability of these important ecosystems. The submergence of these coastal ecosystems will have significant impacts. As our wetland ecosystems become increasingly fragile and vulnerable, an enhanced understanding of changes at the landscape level will be crucial to their preservation.

Faults are found in wetlands along the Gulf Coast region and have been recognized by geologists for many years; however, the use of these faults to study the impacts of elevation and land cover change has yet to be conducted. Faults provide a point of reference to the impacts of RSLR on wetland habitats; they can be used as key geologic reference features in evaluating the impacts of RSLR on local ecosystems. The use of coastal faults in wetlands offers the ability to identify threshold rates of RSLR that can negatively affect wetland sustainability at the landscape scale allowing coastal managers to better be able to manage these important natural resources though mitigation of land loss and coastal change and restoration projects. There has been limited exploration of the spatially-explicit nature of coastal faulting on wetland vegetation and wetland land cover.

Change detection, through remote sensing, senses environmental changes through the use of multiple scenes covering the same geographic area acquired over a

---

This thesis follows the style of *Geocarto International*.

period of time and is useful in many applications including land use and land cover change, habitat fragmentation, coastal change, and urban sprawl. Image processing techniques aid in analyzing the changes within ecosystems of interest. This practice provides scientists the ability to closely monitor and understand the dynamics of landscapes of interest.

A geographical information system (GIS) database quantifies, manipulates, and analyzes the geographic information derived from remote sensing products. The geographic information data is useful for decision making, inventorying the environment, observing change, and prediction based on current situations. This is accomplished through spatial, temporal, and statistical analysis techniques with digital image processing techniques.

The opening objective of this study was to demonstrate and document land cover change within a wetland that results from sea level rise and elevation change over time due to coastal faulting. The closing objective of this study was to simulate land cover conversion as a function of RSLR within a Matagorda, Texas wetland and to compare and contrast the impact of specific rates of both fault-induced elevation change and predicted International Panel on Climate Change (IPCC) sea level rise projections.

2. FAULT-INDUCED WETLAND LOSS AT MATAGORDA, TEXAS, USA: LAND COVER CHANGES FROM 1943 TO 2008

2.1 Introduction

Wetlands perform a variety of essential services for society, including flood control, coastal protection and stabilization, carbon storage, aquifer recharge, water purification and filtration, exportation of nutrients to coastal waters, fish production and biodiversity maintenance (e.g. Richardson 1994, Mitsch and Gosslink 2000b, Keddy 2009). Accelerated sea level rise presents many dangers for coastal wetlands, as well as for the 53% of the U.S. population who live in the coastal zone (e.g. Mitsch and Gosslink 2000a, LaFever *et al.* 2007, Craft *et al.* 2009, Ross *et al.* 2009). The submergence of these coastal ecosystems, where rates of relative sea level rise (RSLR) are greater than rates of vertical accretion, will have significant impacts (Day *et al.* 1995, Jallow *et al.* 1996, Leatherman 2001). Under recent projections, global eustatic sea level rise is expected to increase over the next decade due to global warming (IPCC 2007). An accelerated rate of sea level rise is a threat to the biodiversity within the wetlands, potentially causing ecoregions to shrink, disappear, or fragment (Menon *et al.* 2010). As our wetland ecosystems become increasingly fragile and vulnerable, an enhanced understanding of the impacts of fundamental change at the landscape level is crucial to

---

*Reprinted with permission from "Fault-induced wetland loss at Matagorda, Texas, USA: Land cover changes from 1943 to 2008" by M.D. Cline, R.A. Feagin, K.M. Yeager, and J.M. Van Alstyne, 2011. *Geocarto International*, 26, 633-645, Copyright [2011] by Taylor & Francis.

their preservation.

Faults provide a point of reference to the impacts of RSLR on wetland habitat; they can be used as key geologic reference features in evaluating the impacts of RSLR on local ecosystems. Faults are important geological features in that they allow for the evaluation of potential sea level scenarios, under current conditions and due to natural factors (Morton *et al.* 2000). It has also been proven that surface faults commonly are related to subsurface faults, allowing for the evaluation of subsurface activity (White and Tremblay 1995).

Surface expressions of subsurface faults can be found in wetlands along the Gulf Coast occur for multiple reasons, and their activity can be driven by both natural and anthropogenic processes. Natural processes generally can include the formation and motion of subsurface structures, such as salt bodies and deep growth faults (Salvador 1987, Diegel *et al.* 1995, Dokka *et al.* 2006). In contrast, faulting driven by human activities is generally a result of hydrocarbon production, subsurface water removal, reservoir compaction and reduced sedimentation (White and Tremblay 1995, White and Morton 1997, Hartig *et al.* 2002, Dokka *et al.* 2006, Morton *et al.* 2006, Chan and Zoback 2007, Mallman and Zoback 2007, Morton and Bernier 2010).

Rates of sea level rise and subsidence are likely to affect both vertical accretion of wetland vegetation (Moorhead 1995) and the rate of lateral migration across the landscape (Feagin *et al.* 2010a). According to some studies, human induced subsidence and faulting associated with subsurface fluid withdrawal has accelerated RSLR, impacting coastal erosion rates, and ultimately resulted in the destruction of vital

wetland areas (White and Tremblay 1995, Feagin *et al.* 2005). From an ecological standpoint, RSLR/subsidence can significantly alter the vegetation makeup of wetland communities (White and Morton 1997), can severely hamper the ability of wetlands to fulfill their natural functions, and can affect biodiversity (LaFever *et al.* 2007, Ross *et al.* 2005).

There has been limited exploration of the spatially-explicit nature of coastal faulting on wetland vegetation and wetland land cover. As such, the primary objective of this study was to demonstrate and document land cover change within a wetland that results from sea level rise and elevation change due to coastal faulting. Methods utilized included the classification of aerial photography on both sides of the immediate fault area ranging from 1943 until 2008 into four specific categories: water, low marsh, salt flat, and high marsh. Once complete, a Geographic Information System (GIS) database was used to quantify the amount of change over time for each category of land cover.

2.2 Methods

2.2.1 Study Area

This study area is a salt marsh wetland located on East Matagorda Peninsula, near the town of Matagorda, Texas, USA (Figure 1(a)). The East Matagorda Peninsula is a transgressive barrier island feature that was connected to the mainland in the early 1920s as a result of human modification. The study area lies in the southwestern corner of Matagorda Bay on this peninsula and can be seen in relation to surrounding features in a 1995 SPOT image at 5 m spatial resolution, which delineates the study area as well as the surface expression of the subsurface fault (Figure 1(b)).

The wetland vegetation at this site is comprised of salt marsh plant cover typical for this region, with zonation strongly dependent upon elevation: open water with some *Ruppia maritima* L. and *Halodule wrightii* Asch., low marsh dominated by *Spartina alterniflora* Loisel., mid marsh dominated by *Salicornia virginica* Standl. and *Batis maritima* L., unvegetated salt flat with some *Monanthocloe littoralis* Engelm. around the edges, and high marsh dominated by *Spartina spartinae* (Trin.) Merr. ex Hitchc.

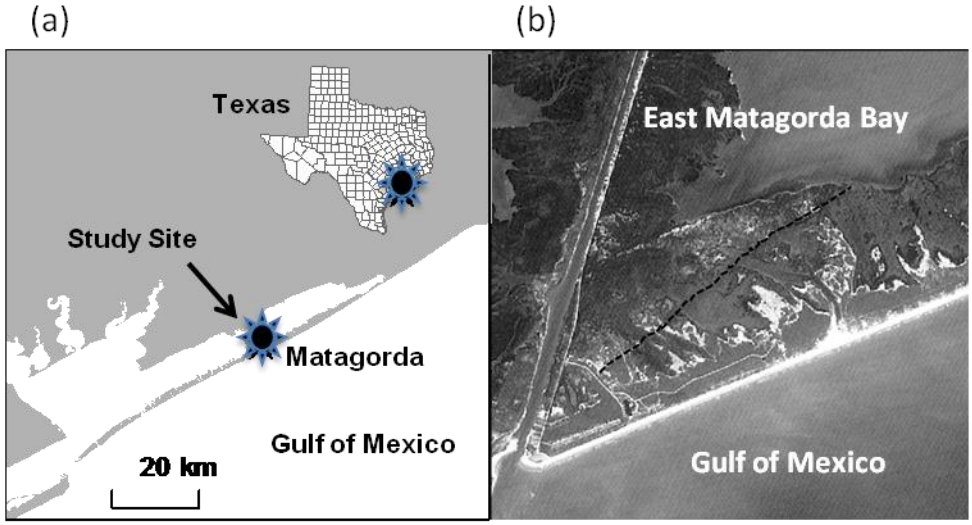

Figure 1. a) Geographic location of the study site on the Texas coast. b) SPOT imagery of the study site in relation to surrounding features in 1995. Delineation of the study area is represented by the solid line and delineation of the surface fault expression is represented by the dashed line.

A normal growth fault bisects our study area (Figure 1(b)). Subsurface seismic imaging, litho- and biostratigraphic contacts, and ground survey datasets have confirmed the presence of this fault (Feagin *et al.* 2010b). Kreitler (1976) traced a possible fault in this location, as an extrapolation of a subsurface fault that stretched several kilometers offshore.

Based upon visual inspection of imagery from 1943, the surface at our study site shows no apparent fault-produced features. By the 1960s and 1970s, exploratory drilling for natural gas and oil was occurring in this region (Railroad Commission of Texas 2011). In an image from 1978, a clear, linear feature can be seen bisecting the study site. In this same image, a drilling rig can be seen and the Railroad Commission of Texas (2011) records a horizontal well at this location, though it was apparently a dry well (no gas found). By the 1980s, natural gas extraction began from a reservoir that was directly adjacent to the subsurface fault described by Kreitler (1976), though 4 km offshore of its surficial expression. Natural gas extraction from this reservoir continued until the early 2000s. Today, extensive natural gas extraction continues from several other reservoirs, located approximately 12 km offshore.

2.2.2 Image Classification and Analysis

A large set of aerial imagery was acquired for the study area. From this set, four images were chosen, one each from 1943, 1978, 1996, and 2008. Images were selected to achieve a representative time sequence over a span of many years, as well as to maximize image quality. The 1943 and 1978 images were black and white. The 1996 and 2008 images were color-infrared (CIR). The 1943, 1978, and 1996 images were acquired at 1 m^2 horizontal resolution. The 2008 image was acquired at 0.1 m^2 horizontal resolution. This 2008 image was then resampled by majority rule to 1 m^2, in order to match the resolution of the other images.

An area of interest (AOI) vector polygon was created within a Geographic Information System (GIS) and all raster images were clipped to its extent (Arc10.0,

ESRI, Redlands, California). The AOI contained a landscape-scale view of both sides of the fault, and extended the length of the fault's expression within the salt marsh.

Each of the four images was then classified in ENVI 4.7 (ITT Visual Information Solutions, Boulder, CO, USA), using the iterative self-organizing data analysis technique (ISODATA) unsupervised algorithm. Thirty spectral classes were initially identified and were then combined into four information classes: water, low marsh, salt flat, and high marsh. Classified images were then smoothed using a 7 x 7 majority filter to remove noise.

Visual inspection of the classified images revealed that this procedure had resulted in several obviously misclassified locations for the 1943 and 1978 data sets. Primarily, this classification method was able to distinguish the differences between water and land; however, it proved unsuccessful at distinguishing differences between land classes. In both black and white images, the classification algorithm was unable to detect subtle differences in shading and apparent reflectance between these surfaces. We initially sought to correct these errors by hand-digitizing the entire set of four images. However, we quickly realized that the landscape in our study area was extremely heterogeneous at a fine scale; there were small patches of the various classes interspersed with one another throughout the AOI. Due to this interspersion, hand digitization required digitizing class-specific polygons within other differing-class polygons. Several levels of embedded polygons-within-polygons were going to be required of this digitization effort. Moreover, digitization would have required that all polygon edges matched the edges of other adjacent polygons, and any small errors

would have added up to significant areas of land when this procedure was iterated across the landscape. We thus felt that a combination procedure was warranted. We chose to use the classified images as the base layer, smoothed them with the 7 x 7 filter to solve a portion of the interspersion problem, and then systematically corrected all apparent errors by hand.

2.2.3 Digitization

In order to capture the detail and heterogeneity of the landscape, the water class polygons produced by the classification were visually inspected for accuracy and then used in the digitized product. The water class polygon was overlaid onto the AOI polygon and then clipped, producing a product containing two classes—water and land. The specific land cover classes were then hand digitized using both the editor and advanced editor toolbars in a GIS, utilizing functions such as creating features, clipping, merging, exploding, cutting, and reshaping (Arc10.0, ESRI, Redlands, California). In order to maintain detail consistency, a constant scale (1:3,000) was used throughout the process and a minimum feature size was established (10 m^2). Land cover type classification was influenced by our knowledge of marsh functions, as well as contrast and spectral differences noted in the imagery. The final outputs included a classified product for the full extent of the landscape, as well as classifications for the upthrown and downthrown extents for the years 1943, 1978, 1996, and 2008.

2.2.4 Data Analysis

The final digitized product resulted in a rich collection of data for analysis (Figure 2). Using the classified image product, areas were calculated using the GIS for

all land cover classes considered. The quantitative area data for each classification type (water, low marsh, salt flat, and high marsh) was extracted using the GIS attribute table and logic statements for the full AOI, and for the upthrown and downthrown extents during each time period.

In order to evaluate the presence of a relationship between subsidence and distance from the fault, class areas were calculated for strips of equal thickness at normal fixed distances from the fault. To accomplish this, a multiple ring buffer geoprocessing technique was applied to the fault location, stretching the length of the fault within the AOI. The upthrown fault strips were located 20 m, 40 m, and 60 m from the fault and the downthrown fault strips identically spaced. Quantitative area data was extracted for all classes, and within each measurement strip, using the methods described above in each 20 m strip.

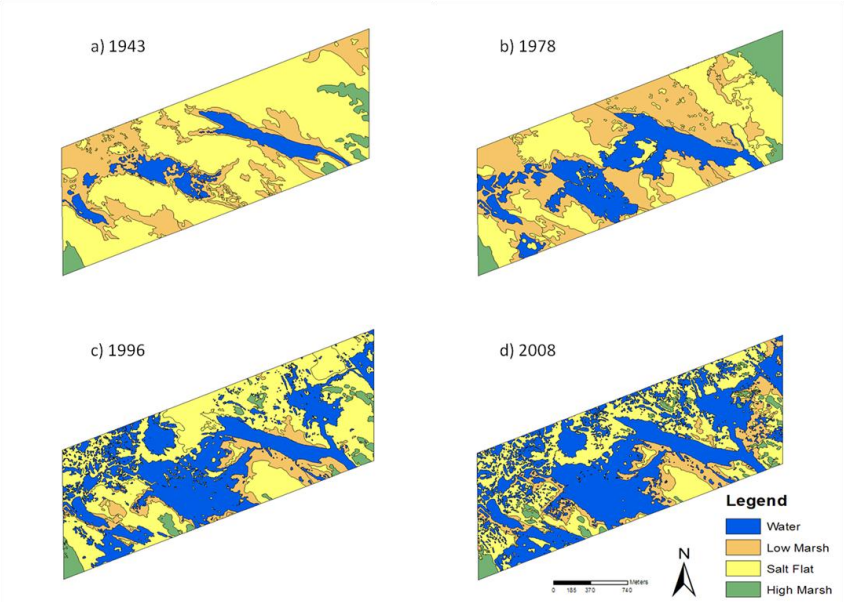

Figure 2. Classified images of the study area located in Matagorda, Texas.

A change detection analysis was conducted from 1943 to 2008 using the classified imagery. This was performed in the GIS by applying the union function to the classified imagery and utilizing the output attribute table and logic statements to extract the necessary quantitative data. This method was applied to the full extent imagery, upthrown and downthrown imagery, as well as the fault strip imagery.

2.2.5 Accuracy Assessment

An accuracy assessment was conducted by collecting 68 in situ ground control points (GCP) in 2011. The in situ data were recorded to a point feature shape file which was then compared to the final classification product using the GIS by extracting the class values to the GCP. These data were then exported to Microsoft Excel in order to generate precise accuracy calculations. Based on the comparison of the GCP to the classified data, a confusion matrix was generated to evaluate the accuracy of the classification. The result of this matrix indicated an overall accuracy of 88.06% and a kappa coefficient of 0.83. The producer accuracies for water, low marsh, salt flat, and high marsh were 95.83%, 70.00%, 100.00%, and 85.71% respectively. Similarly, the user accuracies were 100.00%, 100.00%, 66.67%, and 100.00% for water, low marsh, salt flat, and high marsh respectively. The errors of omission for water, low marsh, salt flat, and high marsh were 4.17%, 30.00%, 0.00%, and 14.29% while the errors of commission were 0.00%, 0.00%, 33.33%, and 0.00% respectively.

2.3 Results

2.3.1 Full Extent

The full extent of the study area is approximately 373 ha. From 1943 to 2008, a significant decrease in the total area of land can be seen (Figure 3(a)). Land accounted for 337.7 ha of the AOI in 1943, and 197.5 ha in 2008. This decrease in land area was inversely proportional to the increase in water area. Over this time, shifts in land cover classes can also be noted (Figure 3(b)). An overall decrease in the total area of low marsh is demonstrated with 100.1 ha of low marsh in 1943, and 50.3 ha in 2008. Similarly, salt flats also experienced a net decrease in total area, with 222.5 ha in 1943, and 133 ha in 2008. The high marsh class remained relatively constant over the time range of interest, with 14.9 ha in 1943, and 14.2 ha in 2008; however, area fluctuations did occur.

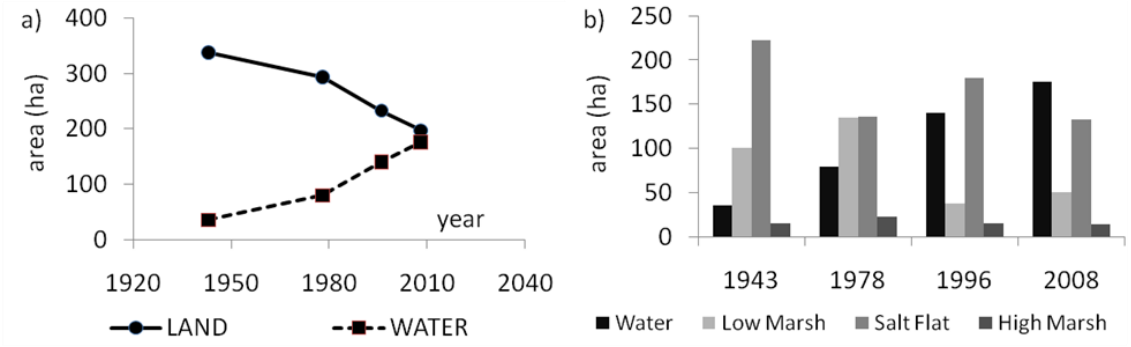

Figure 3. a) Line graph displaying transition of land area loss and water area gain from 1943 to 2008 in ha. b) Bar graph displaying transition of specific land cover classes in 1943, 1978, 1996, and 2008 in ha.

2.3.2 Upthrown Extent

The upthrown extent of the AOI is approximately 160 ha. From 1943 to 2008, a decrease in the total area of land can be seen (Figure 4(a)). Land accounted for 145.5 ha

of the upthrown extent in 1943 and 99.7 ha in 2008. With the decrease in land area, a simultaneous increase in water area occurred. Over this time, shifts in land cover classes can also be noted (Figure 4(c)). An overall decrease in the total area of low marsh was observed, with 52.7 ha of low marsh in 1943, and 8.6 ha in 2008. Salt flats remain relatively constant over the time of interest, with 90.2 ha in 1943 and 84.1 ha in 2008; however, area fluctuations did occur. The high marsh class experienced an overall increase in total area, with 2.8 ha in 1943 and 6.9 ha in 2008.

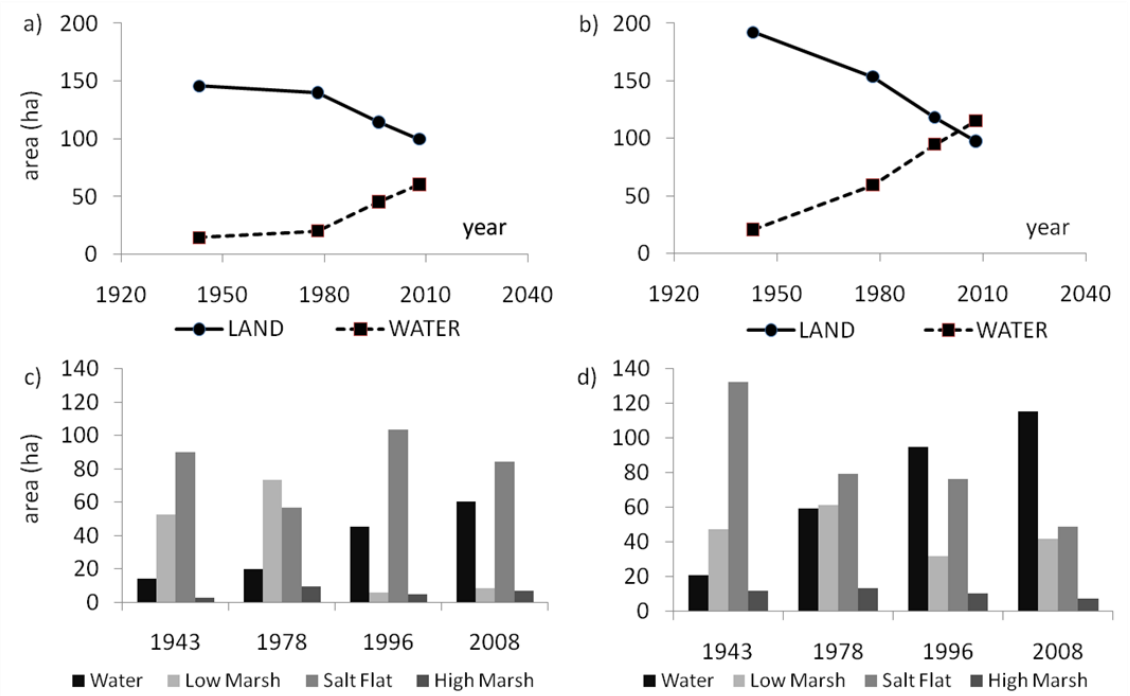

Figure 4. Line graphs displaying transition (in ha) from 1943 to 2008 of a) upthrown land area loss and upthrown water area gain; and b) downthrown land area loss and downthrown water area gain. Bar graphs displaying transition of specific land cover classes (in ha) in 1943, 1978, 1996, and 2008 c) within the upthrown extent; and d) within the downthrown extent.

2.3.3 Downthrown Extent

The downthrown extent of the AOI is approximately 213 ha. From 1943 to 2008, a decrease in total land area can be seen (Figure 4(b)). Land accounted for 192.1 ha of the downthrown extent in 1943, and 97.8 ha in 2008. The decrease in land area was matched by an increase in water area. Over this time, shifts in land cover classes can also be noted (Figure 4(d)). Low marsh remained relatively constant over the time range of interest, with 47.6 ha in 1943, and 41.7 ha in 2008; however, area fluctuations did occur. Salt flats experienced an overall decrease in total area, with 132.3 ha in 1943, and 48.9 ha in 2008. The high marsh class revealed a small net decrease in the total area, with 12.2 ha in 1943, and 7.2 ha in 2008.

2.3.4 Change Detection Analysis

The change detection analysis from 1943 to 2008 demonstrates shifts in land cover classes within both the upthrown and downthrown extents (Figure 5).

Within the upthrown extent, water increased significantly in area, with 16.2 ha of low marsh and 30.3 ha of salt flat converting to water. Significant low marsh trends included a 16.2 ha conversion to water, and a 29.9 ha conversion to salt flat. Minimal amounts of water and salt flat converted to low marsh over time, resulting in a significant loss for total area of low marsh during this time period. Notable trends within the salt flat class included a 30.3 ha conversion to water; however, 29.9 ha of low marsh converted to salt flat, resulting in minimal net change from 1943 to 2008 (Figure 4(c)). Within the high marsh class, a 0.4 ha conversion to salt flat was observed;

however, 1.9 ha of low marsh and 2.6 ha of salt flat converted to high marsh, leading to a net increase in high marsh from 1943 to 2008.

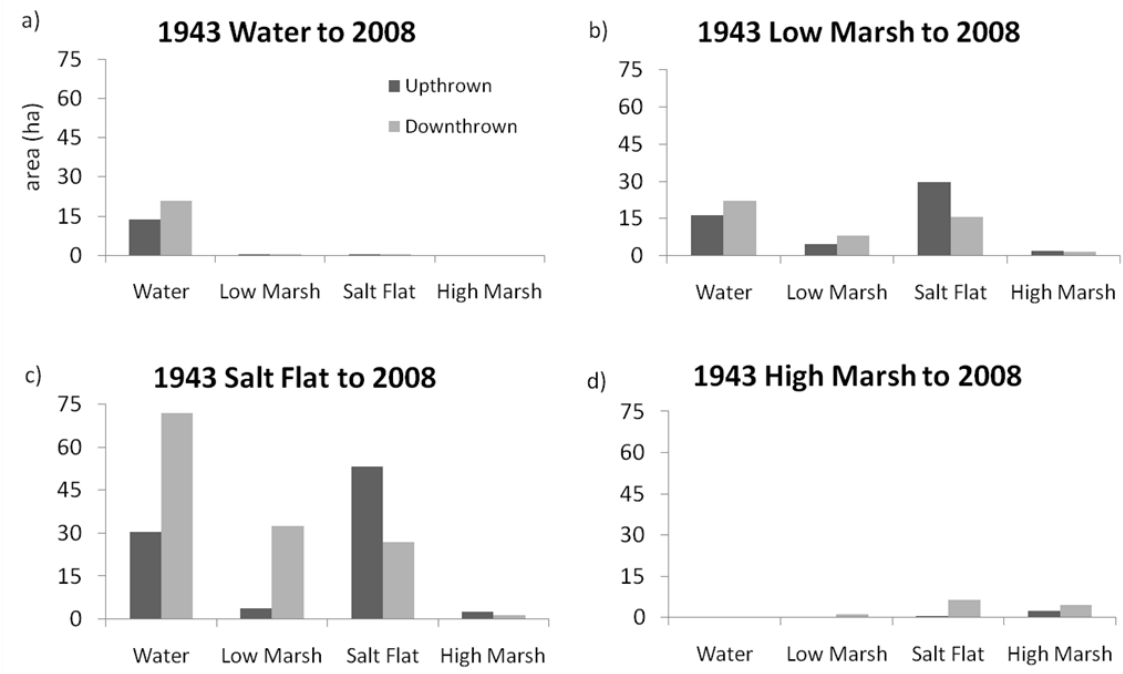

Figure 5. Display of from-to change analysis (1943 to 2008, in ha) for (a) water area, (b) low marsh area, (c) salt flat area, and (d) high marsh area.

In the downthrown extent, water experienced a significant increase, with 22.3 ha of low marsh, 71.8 ha of salt flat, and 0.2 ha of high marsh converting to water. Relevant low marsh trends included a 22.3 ha conversion to water, and a 15.7 ha conversion to salt flat; however, 32.4 ha of salt flat converted to low marsh, resulting in minimal net change from 1943 to 2008 (Figure 4(d)). Significant trends within the salt flat class included a 71.8 ha conversion to water, and a 32.4 ha conversion to low marsh, with only 15.7 ha of low marsh and 6.3 ha of high marsh converting to salt flat, resulting in a significant net decrease in salt flat area by 2008. Notable trends within the high

marsh class included a 1.3 ha conversion to low marsh, and a 6.3 ha conversion to salt flat, with minimal conversion of other classes to high marsh, resulting in a net decrease in high marsh from 1943 to 2008.

2.3.5 Fault Strips

The upthrown fault strips, occurring at 20 m, 40 m, and 60 m from the fault, account for 8 ha, 7.8 ha, and 7.7 ha respectively. Similarly, the downthrown strips occurring at 20 m, 40 m, 60 m, and 80 m from the fault, account for 8 ha, 7.8 ha, 7.6 ha, and 7.5 ha, respectively. Over the time interval from 1943 to 2008, two important observations are made. Specifically, land losses are greater on the downthrown versus the upthrown side of the fault, and land losses on either side of the fault decrease as distance from the fault increases (Figure 6).

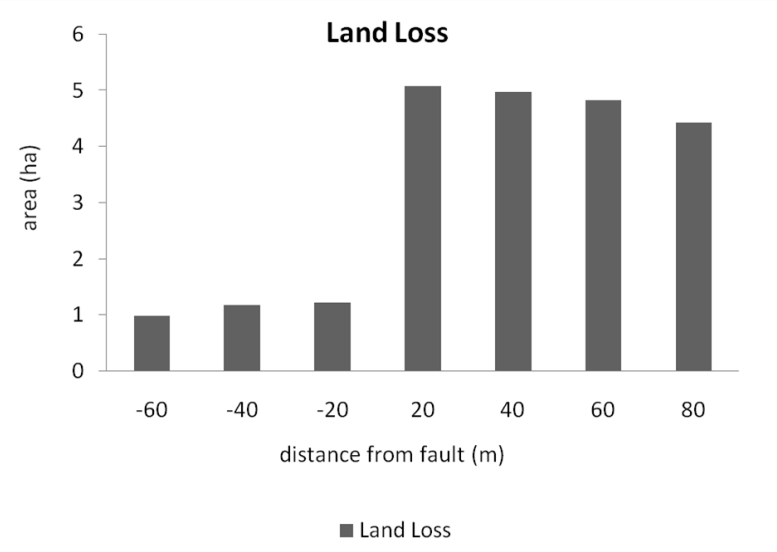

Figure 6. Change of area (ha) between 1943 and 2008 at designated distances from the fault in 20 m strips, with 0 m representing the fault trace at the surface. Positive and negative values on the x-axis represent increasing distances from the fault trace on the downthrown, and upthrown sides, respectively.

2.4 Discussion

This study presents evidence of significant changes in wetland land cover classes over time. From 1943 to 2008, a shift in water and land area was notable, with water increasing and land decreasing at the landscape scale across the AOI. By examining these results independently within the upthrown and downthrown extents, the effects of differential subsidence can be visually observed. The shifts in land cover classes on the downthrown extent were both more rapid and greater in magnitude as compared to those on the upthrown extent.

Transitions between specific land cover classes were also observed, primarily within the low marsh and salt flat classes. Within the upthrown extent, as water increases, low marsh largely overtakes salt flat; however, this encroachment results in very little expansion of salt flat at the expense of high marsh. Within the downthrown extent, as water increases, salt flat and low marsh areas are re-distributed, with some salt flat area transitioning to low marsh and an even larger portion of low marsh transitioning into salt flat. Once more, these shifts elicit little change with respect to the area occupied by the high marsh class. These shifts in land cover class were further examined proximal to the fault scarp. As distance from the fault decreases, these effects also decrease, indicating greater activity at the fault location.

Wetland land cover classification is often a challenge due to the complexity of wetland landscapes and the influence of biophysical variables such as water levels, salt content, phonological vegetation variations, and density (Zhang *et al.* 2011). The historical dates used in this study presented multiple challenges in regards to

classification methods, further compounding the complex nature of land cover classification in wetlands. Manual image interpretation of aerial photography has been used to map landscape features and identify wetlands since the 1930s and is still considered useful, producing high quality, detailed maps (Ozesmi *et al.* 2002, Halabisky *et al.* 2011). However, due to the time consuming nature of the method, it would be beneficial to explore computerized classification methods. Due to the nature of the dataset used in this study, texture transformation extraction as presented by Irons and Petersen (1981) would be a beneficial addition to the imagery for the classification process. In addition, a method utilizing an object-oriented classifier similar to that presented by Halabisky *et al.* (2011) could prove to be beneficial, as could the use of advanced, nonparametric classifiers (Baker *et al.* 2006), which could further improve wetland vegetation classification performance. Due to the inherent value that wetlands contribute to coastal ecosystems, and the extensive technology now available, further inquiry into the application of remote sensing techniques with respect to wetland classification would provide significant benefit to researchers across a broad range of disciplines.

3. MODELING RELATIVE SEA LEVEL RISE IN COASTAL WETLANDS: GROWTH FAULT MOVEMENT AS A PROXY FOR UNDERSTANDING THE IMPACT OF CLIMATE CHANGE

3.1 Introduction

Accelerated sea level rise presents many dangers for coastal wetlands, as well as for the 53% of the US population who live in the coastal zone (e.g. Mitsch and Gosslink 2000a, LaFever *et al.* 2007, Craft *et al.* 2009, Ross *et al.* 2009). The submergence of these coastal ecosystems through relative sea level rise (RSLR), where rates of eustatic water level rise and subsidence are greater than rates of vertical accretion, will have significant negative ecological impacts (e.g. Day *et al.* 1995, Jallow *et al.* 1996, Leatherman 2001). By identifying threshold rates of RSLR that can negatively affect wetland sustainability at the landscape scale, coastal managers may be better able to manage these important natural resources.

RSLR can be due to subsidence, and this component of relative elevation change can be associated with growth fault activity, particularly on the US Gulf Coast (White and Tremblay 1995; White and Morton 1997). Surface expressions of subsurface faults can be found in Gulf Coast wetlands and their activity can be driven by both anthropogenic and natural processes. Faulting driven by human activities is generally a result of hydrocarbon production, subsurface water removal, and reservoir compaction (White and Tremblay 1995, White and Morton 1997, Hartig *et al.* 2002, Dokka *et al.* 2006, Morton *et al.* 2006, Chan and Zoback 2007, Mallman and Zoback 2007, Morton

and Bernier 2010). These human activities may be overlain on top of natural processes that formed the pre-existing subsurface structures that are subject to motion, typically at longer time scales, such as salt bodies and deep growth faults (Salvador 1987, Diegel *et al.* 1995, Dokka *et al.* 2006).

RSLR can also be due to eustatic water level change. Under the most recent Intergovernmental Panel on Climate Change projections, global eustatic sea level is expected to rise and accelerate over the next century due to global warming (IPCC 2007). An accelerated rate of sea level rise will present a further threat to the biodiversity with the wetlands, potentially causing ecoregions to shrink, disappear or fragment (Menon *et al.* 2010).

Accordingly, modeling has been an area of interest to quantify the potential impacts of RSLR on coastal ecosystems (Costanza *et al.* 1990, Titus and Richman 2001). These models often employ digital elevation models (DEMs) in conjunction with geographic information system (GIS) technology to model RSLR in coastal areas (Hennecke and Cowell 2000, LaFever *et al.* 2007, Snow and Snow 2009, Feagin *et al.* 2010*a*) at both large scales (Thieler and Hammar-Klose 2000, McFadden *et al.* 2007) and small scales (Lee *et al.* 1992, Craft *et al.* 2009). There are several other documented approaches to evaluating RSLR in wetlands. One such method is to measure nitrogen, salinity, and biomass readings to provide an accurate evaluation of saltwater encroachment (Craft *et al.* 2009). Markov chain analysis and cellular automaton have been used to project future land cover change as well (Shirley and Battaglia 2008, Ross *et al.* 2009). Regression modeling and extrapolation techniques incorporating output

from sea level modeling, IPCC predictions, and local tide gauges in conjunction with plausible accretion rates have also been used to project RSLR at broad scales (Titus & Richman 2001, Hartig *et al.* 2002). Fine-scaled GIS-based terrain analysis and geostatical techniques have been used to provide quantitative data and spatially explicit visualization of complex ecological patterns and processes occurring in coastal dunes (Kim *et al.* 2008). In addition, simulation modeling of hydrology, topography, nutrient biogeochemistry, and community dynamics has been used to forecast the structure and function of a landscape and its response to changes (Twilley and Rivera-Monroy 2005). Simulation techniques have also been utilized to project RSLR (Yin *et al.* 2010), as well as the importance and influence of barrier island relative location on esturine ecosystems (Reyes *et al.* 2005). Still, no work has predictively modeled the impact of growth fault movement on wetlands, or applied multiple RSLR rates differentially across a single landscape.

The primary objective of this study was to simulate land cover conversion as a function of RSLR within a Matagorda, Texas wetland. The secondary objective was to compare and contrast the impact of specific rates of both fault-induced elevation change and predicted IPCC sea level rise projections. To accomplish these objectives, land cover classes were first identified as water, tidal wetland, and non-tidal wetland, and a GIS model was then constructed to quantify the amount of expected change in the wetland given specific RSLR rates.

3.2 Methods

3.2.1 Study Area

This study area is a salt marsh wetland located on East Matagorda Peninsula, near the town of Matagorda, Texas, USA (Figure 7(a)). The East Matagorda Peninsula is a transgressive barrier island feature that was connected to the mainland in the early 1920s as a result of human modification. The study area lies in the southwestern corner of Matagorda Bay on this peninsula and can be seen in relation to surrounding features in this 1995 SPOT image at 5 m spatial resolution. A growth fault bisects the study area (Figure 7(b)). Subsurface seismic imaging, litho- and biostratigraphic contacts, and ground survey datasets have confirmed the presence of this fault (Feagin *et al.* 2012). Kreitler (1976) traced a fault in this location, as an extrapolation of a subsurface fault that stretched several kilometers offshore.

The wetland vegetation at this site is comprised of salt marsh plant cover typical for this region, with zonation strongly dependent upon elevation: open water with some *Ruppia maritima* L. and *Halodule wrightii* Asch., low marsh dominated by *Spartina alterniflora* Loisel., mid marsh dominated by *Salicornia virginica* Standl. and *Batis maritima* L., unvegetated salt flat with some *Monanthocloe littoralis* Engelm. around the edges, and high marsh dominated by *Spartina spartinae* (Trin.) Merr. ex Hitchc.

3.2.2 Imagery and Classification of Vegetation Zones

A classified image, originally developed in Cline *et al.* (2011) as based on 2008 aerial photography, was acquired for the study area. This classified image was of 1 m horizontal resolution, clipped to an area that gave a landscape-scale view of both sides of

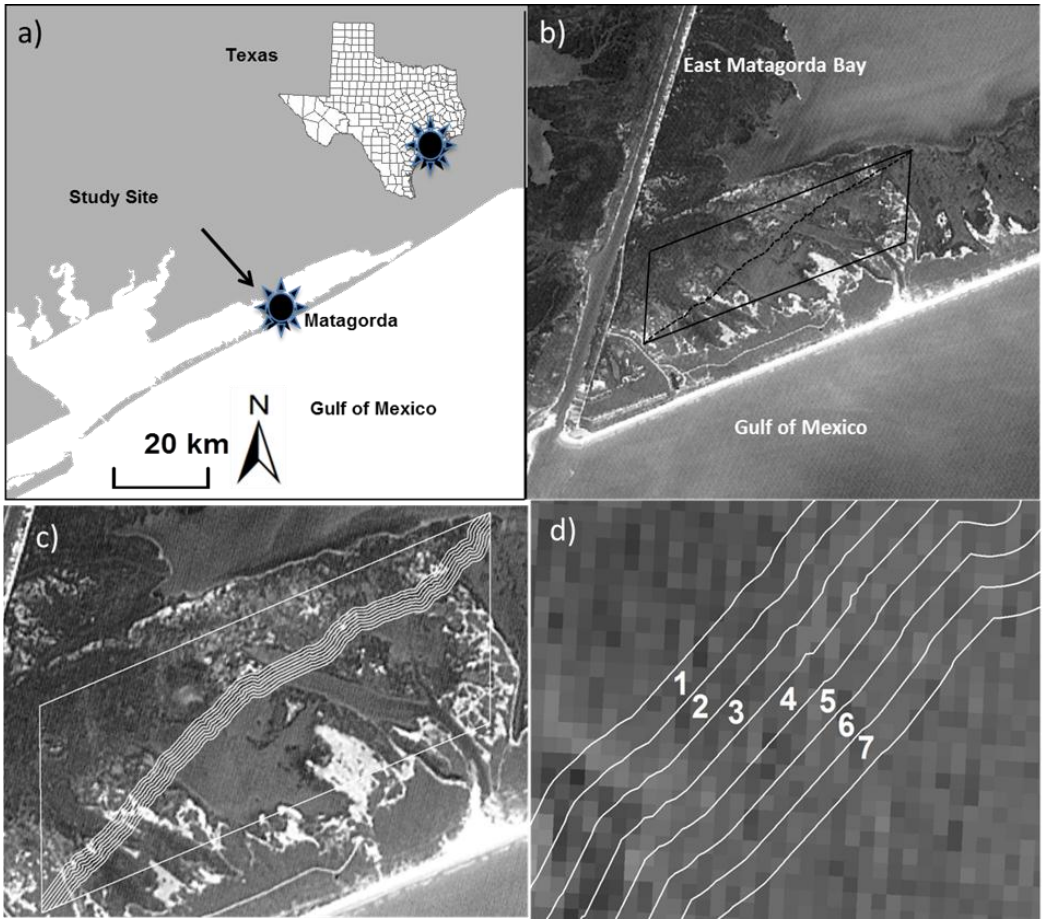

Figure 7. (a) Geographic location of the study site on the Texas coast. (b) SPOT imagery of the study site in relation to surrounding features in 1995. Delineation of the study area is represented by the solid line and delineation of the surface fault expression is represented by the dashed line. (c) fault strip locations in relation to the study area and the surface expression of the fault. (d) fault strip numbers 1-7, as described in the text and Table 1.

the fault and extended the length of the fault's surface expression within the salt marsh, and had an overall classification accuracy of 88.06% and kappa coefficient of 0.83 (Cline *et al.* 2011). A 2008 light detection and ranging (LiDAR) dataset was then acquired for this same area from the Texas Natural Resource Information System (TNRIS). TNRIS had converted the original point cloud data from .LAS file format into a DEM with 1 m horizontal resolution and 0.01 m of vertical resolution.

3.2.3 Elevation Range Definition of the Zones

The elevation ranges of the existing vegetation zones were defined by overlaying the LiDAR DEM with the 2008 classified image. To accomplish this, the DEM was vertically sliced every 0.01 m using the spatial analysis and raster calculator tools in ArcGIS 10.0 (ESRI, Redlands, CA, USA). The area of each vegetation zone on the classified image that fell within each DEM slice was then recorded, and summarized in order to create a frequency distribution (Figure 8). Due to the tidal nature of the study area and the interests of the study, we combined all low marsh, mid marsh, and salt flat vegetation zones into a single zone (tidal wetland) and the high marsh vegetation zone was considered separately (non-tidal wetland).

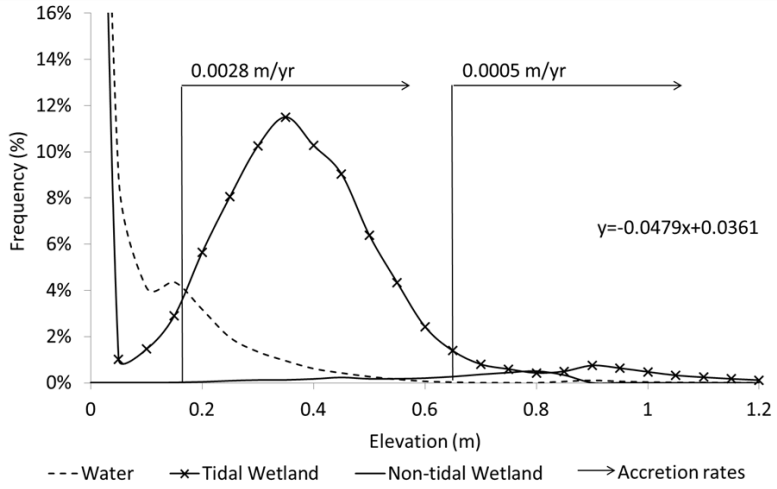

Figure 8. The frequency distribution of each vegetation zone with respect to elevation.

Using the defined elevation ranges, the DEM was then converted into a classified map, where each pixel was classified to a specific zone based upon their ranges. The

final elevation ranges of the zones of interest were defined as: water < 0.17 m; 0.17 m ≤ tidal wetland < 0.65 m; and non-tidal wetland ≤ 0.65 m.

3.2.4 Accretion

Multiple sediment cores were collected at the site as described in Feagin *et al.* (2012), and analyzed for 210Pb and 137Cs radioisotope reactivity to quantify marsh accretion rates at centennial and decadal time scales. In these cores, the maximum average accretion rate was 0.28 cm/yr in the lowest elevations of the tidal wetland. The minimum accretion rate was recorded from the highest elevations of the tidal wetland zone at 0.05 cm/yr. Using this data as a guide, a linear decrease from 0.28 cm/yr to 0.05 cm/yr was calculated and assumed across the tidal wetland class, while the non-tidal wetland class was assumed to have a constant accretion rate of 0.05 cm/yr (Figure 8).

3.2.5 Fault Strips

Multiple sediment cores were collected at the site at 20 m intervals along transects that ran perpendicular to the fault, as described in Feagin *et al.* (2012). In accordance with these 20 m intervals, strips were created within the GIS using the multiple ring buffer tool, with the surface expression of the fault as the buffered feature. The location of each fault strip from the surface fault expression was thus concordant with this set of coring data (Figure 7(c-d)).

To obtain the average annual rate of vertical movement within each fault strip (Table 1), we measured lithostratigraphic offsets in the field coring data, and divided these offsets by the number of years since apparent fault activation. More specifically, we quantified the relative vertical offset in a distinct clay-to-sand layer contact several

meters down core, in North American Vertical Datam of 1988 (NAVD88) units, among the cores that were arrayed perpendicular to the fault plane (Feagin *et al.* 2012). We then divided offsets by 40, the time in years between apparent fault activation and core extraction. These displacement quantities were then vertically referenced relative to fault strip 3, which is immediately on the upthrown side of the fault plane, given the assumption that this location was relatively stationary in global vertical datum units, relative to on-going changes in sea level. The choice of this reference location was based on a relatively low rate of land cover change over ~70 year period in this fault strip (Cline *et al.* 2011), field site inspection of modern day vegetation distributions relative to elevation, and three years of survey grade global positioning system (GPS) data along multiple transects detailing a lower rate of movement in this strip than in the other fault strip locations. This procedure yielded annual rates of RSLR within each strip, as based on the previous 40 years of fault movement.

Table 1. Fault strip reference numbers with location proximal to fault location and vertical fault strip movement rate.

Fault Strip #	Strip Location Relative to Fault	Vertical Movement Downward (cm/yr)
1	40-60 m NW	-0.156
2	20-40 m NW	0.411
3	0-20 m NW	-0.400
4	0-20 m S	0.400
5	20-40 m S	1.167
6	40-60 m S	0.733
7	60-80 m S	1.856

3.2.6 RSLR Simulation

To predict future vegetation distribution under a regime of continued faulting, each fault strip was individually modeled using the average annual rate of vertical movement. In order to implement one time step (10 years), the following formula was calculated at each pixel:

$$e_{i+1} = e_i + a_i - r_i$$

where *e* is the elevation, *a* is the accretion rate based on vegetation type and elevation, *r* is the projected vertical movement of the landscape within a strip, and *i* is the time step. Each scenario began from the initial classified map created from the original DEM. Each pixel was then evaluated by its elevation value and classed based on the elevation ranges of each zone. At each time step, the elevation value of each pixel was adjusted according to the calculation of the equation above. Maps were created after 4 time steps for a 40 year projection (year 2050) and after 9 time steps for a 90 year projection (year 2100).

In order to further examine the effects of subsidence at the landscape scale, the fault strip rates were then individually applied to the study area as a whole (simulating a homogeneous rate of vertical movement across the entire landscape, with movement quantity equal to a given fault strip rate). Each of these rates was applied to the entire study area in the absence of any other component of RSLR. This provided the ability to examine the effect of relative elevation change on the land cover classes at the landscape scale.

Separate simulations were then conducted across the entire landscape for 3 different IPCC (2007) scenarios and 1 additional scenario based on projections in Rahmstorf *et al.* (2007). These 4 scenarios include a low rise of 0.18 m by 2100, a mid rise of 0.39 m by 2100, a high rise of 0.59 m by 2100, and a more extreme rise of 1.40 m by 2100. In these scenarios, *r* in the RSLR simulation equation represented the projected global eustatic sea level rise rate. No fault movement was simulated on top of these rates.

To verify the model, a reverse modeling procedure was run to hindcast our 2008 classification results to our 1943 classification results. The forecast version of the model utilized the current time step elevation and accretion rate data to calculate the next time step elevation; in other words, the current time step accretion rate is dependent upon the previous time step accretion rate. When running in reverse to hindcast, the model was unable to properly evaluate and apply accretion rates due to the change in evaluation direction and was, therefore, applying the incorrect accretion rate to the current time step evaluation. The hindcast resulted in a relatively poor approximation of the 1943 classification results.

3.3 Results

Fault movement changed the wetland land cover. Compared to the 2008 map (Figure 9(a)), the differential fault movement simulation for 2050 (Figure 9(b)) demonstrated notable changes proximal to the fault. In areas where the fault dropped, the tidal wetland class converted to water, yet the non-tidal wetlands were minimally affected. Due to the uplift of the fault in two of the strips on the upthrown side, water

converted into tidal wetland, and tidal wetland converted into non-tidal wetland. Locations outside of the seven strips did not change in this simulation.

The effects of faulting were further examined by applying a single strip rate over the entire landscape. When fault strip rate 1 (-0.156 cm/yr) was applied to the entire landscape, by 2050 the tidal wetland expanded into water, while the non-tidal wetland zone was minimally affected (Figure 10(a)). By 2100, more tidal wetland expanded into water (Figure 10(b)). The landscape responded in a similar manner to fault strip rate 3 (-0.400 cm/yr), though with even more expansion of both tidal and non-tidal wetlands (Figure 10(e), 10(f)).

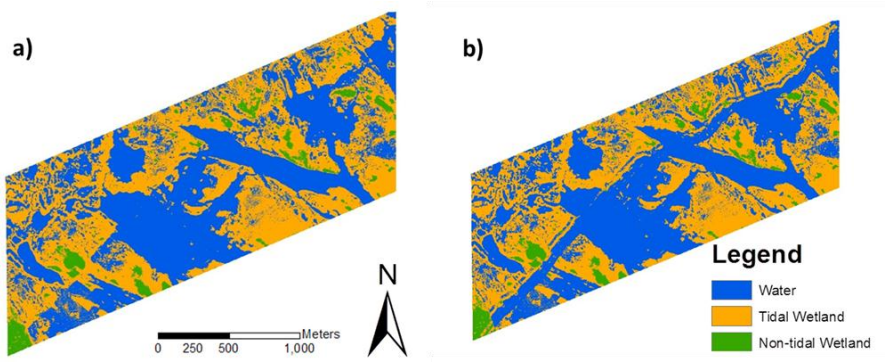

Figure 9. (a) Vegetation zone distribution in 2008, as based on the classified LIDAR data (b) Predicted vegetation zone distribution in 2050.

When fault rate 2 (0.411 cm/yr) was applied to the entire landscape, by 2050 the non-tidal wetland was apparently unaffected while the majority of tidal wetland was inundated by water, leaving fragmented remnants of this zone (Figure 10(c)). By 2100, the tidal wetland was nearly completely inundated by water, leaving only the non-tidal wetland, which experienced a minimal conversion into tidal wetland (Figure 10(d)).

Under the constraints of fault rate 4 (0.400 cm/yr), by 2050 the tidal wetland was significantly inundated by water and non-tidal wetland experienced a slight expansion (Figure 10(g)). By 2100, the tidal wetland was nearly completely consumed by water, leaving only the non-tidal wetland, which experienced an expansion (Figure 10(h)).

When fault rate 5 (1.167 cm/yr), fault rate 6 (0.733 cm/yr), and fault rate 7 (1.856 cm/yr) were applied to the entire landscape through the year 2050, the water increasingly inundated the existing tidal wetland with losses accordant to each rate. Non-tidal wetland also experienced a decrease (Figures 10(i), 10(k), 10(m)). By 2100, water completely inundated the existing tidal wetlands. Non-tidal wetlands significantly decreased. The encroachment of water on the non-tidal wetland converted some non-tidal wetland to tidal wetland for the lower rate; however, for the highest rate of fault strip 7, water had completely inundated the landscape (Figures 10(j), 10(l), and 10(n)).

For the projected eustatic rise scenarios, the IPCC low scenario map was significantly altered by 2050 and 2100 (Figures 11(a), 11(b), respectively) when compared with the 2008 map (Figure 9(a)). The tidal wetlands throughout the area were overcome by water and created an irregular and fragmented landscape. The non-tidal wetlands were minimally affected. The IPCC mid and high scenarios consumed the majority of tidal wetlands; while the non-tidal wetlands began to experience a transition to tidal wetlands (Figures 11(c)-11(f)). The more extreme scenario consumed all of the

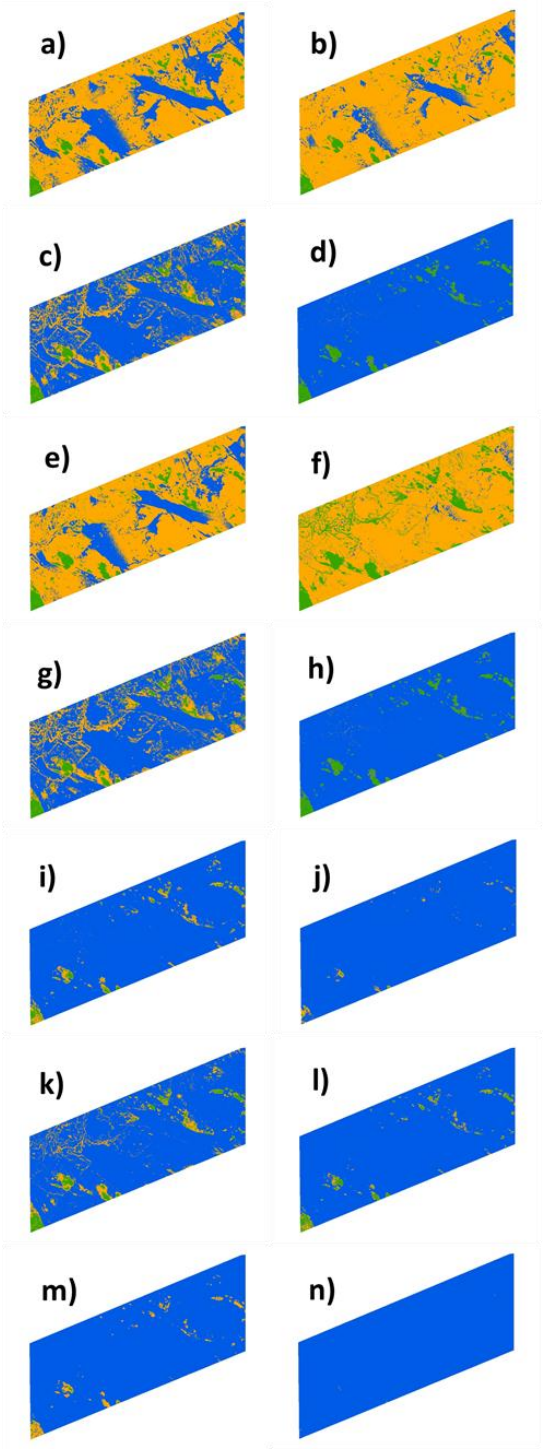

Figure 10. Predicted vegetation zone distribution, assuming the following conditions implemented across the entire landscape: (a) fault strip 1 rate in 2050, (b) fault strip 1 rate in 2100, (c) fault strip 2 rate in 2050, (d) fault strip rate 2 in 2100, (e) fault strip 3 rate in 2050, (f) fault strip 3 rate in 2100, (g) fault strip 4 rate in 2050, (h) fault strip 4 rate in 2100, (i) fault strip 5 rate in 2050, (j) fault strip 5 rate in 2100, (k) fault strip 6 rate in 2050, (l) fault strip 6 rate in 2100, (m) fault strip 7 rate in 2050, and (n) fault strip 7 rate in 2100. North is to the top of each image. Relative scale and color legend is the same as Figure 9.

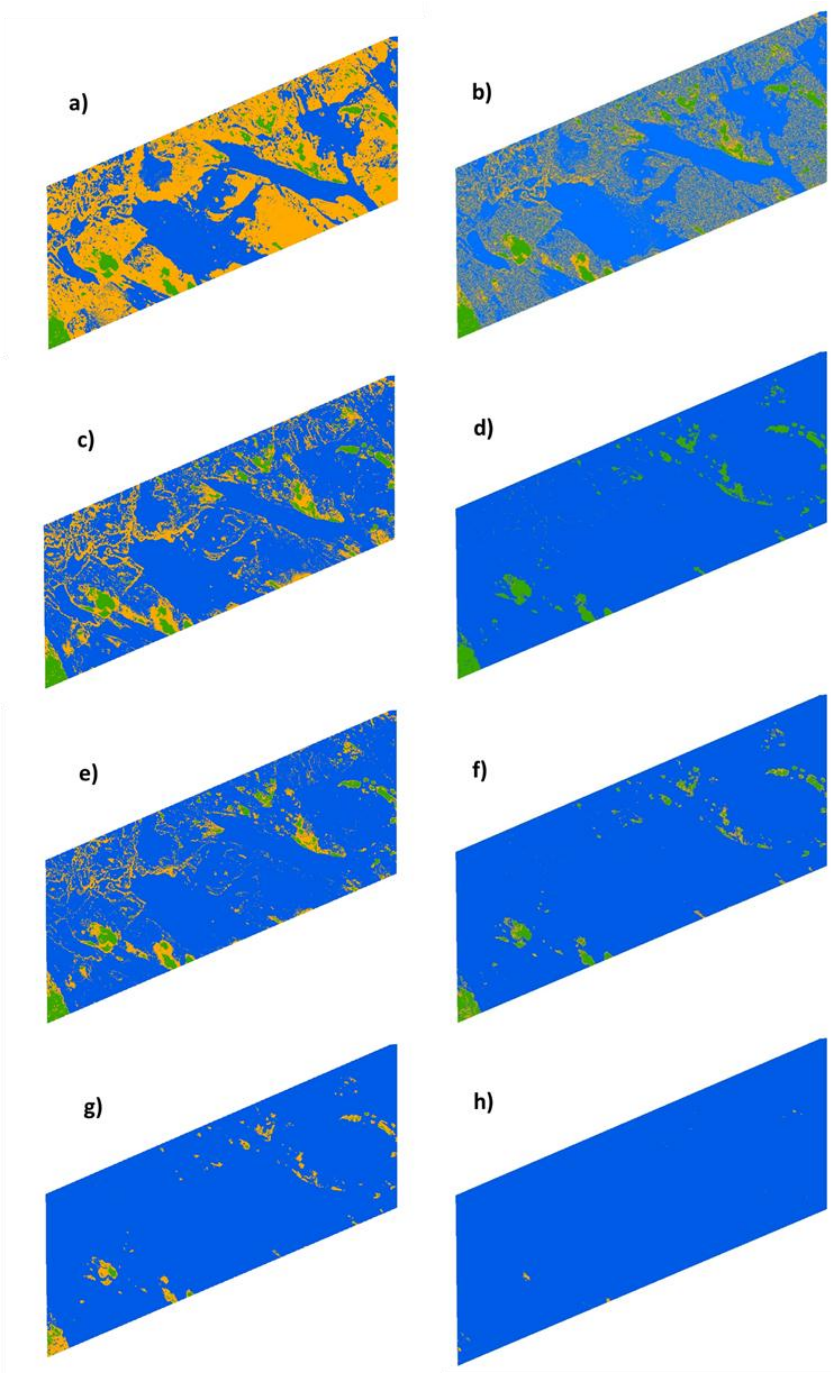

Figure 11. Predicted vegetation zone distribution assuming the: (a) IPCC low scenario 0.18 m) in 2050, (b) IPCC low SLR scenario (0.18 m) in 2100, (c) IPCC mid SLR scenario (0.39) in 2050, (d) IPCC mid SLR scenario (0.39) in 2100, (e) IPCC high SLR scenario (0.59) in 2050, (f) IPCC high SLR scenario (0.59) in 2100, (g) an extreme SLR scenario (1.4 m) after in 2050, and (h) an extreme SLR scenario (1.4 m) in 2100. Map orientation, scale, and legend features are consistent to that of Figure 9. North is to the top of each image. Relative scale and color legend is the same as Figure 9.

tidal and non-tidal wetlands, leaving only the highest elevation non-tidal wetlands to remain which were converted to tidal wetlands (Figures 11(g), 11(h)).

The quantity of tidal marsh loss was positively related to the quantity of decrease in elevation (Figure 12). This relationship held for both eustatic rise projections and fault-induced elevation changes that were homogeneously implemented across the entire landscape. With RSLR, or a relative dropping of the landscape relative to water level, tidal marsh coverage decreased. With relative uplift implemented across the entire landscape, tidal marsh coverage increased.

3.4 Discussion

Rapid water level rise can force tidal wetlands to convert into open water, regardless of whether this relative rise is caused by vertical fault displacement or eustatic sea level rise. Our research shows a threshold relative rise rate of approximately 0.400 cm/yr for a near-complete loss of the Matagorda wetland by the year 2100. This threshold is based on our model of tidal wetland conversion, and is ultimately tied to field data collected from fault strip 4, which is the portion of the landscape that sits immediately to the southeast of the fault line itself. As can be seen in historical imagery of this portion of the landscape (Cline *et al.* 2011) and the modern day wetland-to-open water edge that is present along the fault line, the elevation change rate within fault strip 4 has been enough to convert tidal wetland coverage into open water.

The inflection point in Figure 12(a) for the 2050 projection, at which tidal wetland losses began to accelerate, occurred between the IPCC 2007 low and mid projections. This inflection point generally coincides with RSLR rates of approximately

0.30 cm/yr. Historical tide gauge records from Freeport (0.96 cm/yr), Galveston (0.65 cm/yr), and Rockport (0.49 cm/yr) all exceed this value. Indeed, this section of the Gulf

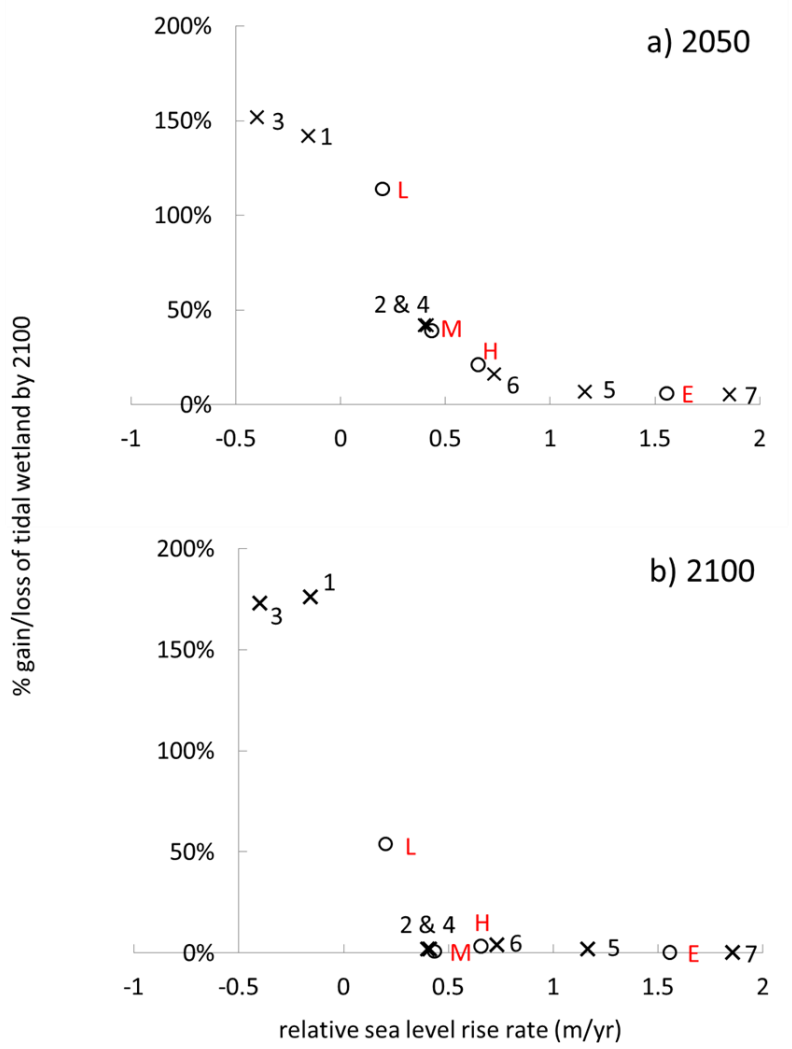

Figure 12. Percent conversion of tidal wetland (gains exceed 100%, losses are less than 100%) into open water, as a function of RSLR for all scenarios, for the years (a) 2050, and (b) 2100. Numerical labeled data points refer to fault strip rates of vertical change (see Table 1 and Figure 10). For alpha labeled data points: L is IPCC low scenario, M is IPCC mid scenario, H is IPCC high scenario, and E is the more extreme Rahmstorf *et al.* (2007) scenario.

Coast has experienced great amounts of tidal wetland loss. Considering the relatively high organic production of herbaceous wetland grasses such as *Spartina alterniflora* in this region due to a warm temperate climate, relatively high amounts of rainfall and nutrient-rich soils, the long-term outlook for other regions with similar wetland species is not good for RSLR rates above 0.30 cm/yr.

We contend that faults can provide a key point of reference to understanding the impacts of climate-induced RSLR on wetland habitat. In our study, fault strips 1 and 3 increased tidal wetland cover, and fit along the curve above the IPCC low scenario. Strips 2 and 4 best approximated the IPCC mid scenario, while strip 6 roughly accorded with the IPCC high scenario. Strips 5 and 7 bounded the Rahmstorf *et al.* (2007) more extreme scenario. In the future, studies could investigate the long-term ecological response of plants in different portions of an elevation-variable, faulted landscape.

Faulting, and more generally RSLR, is likely to affect vertical accretion and sedimentation. Indeed, we have quantified accretion rates as a function of differential fault throw in cores in these same fault strips, in related work (Feagin *et al.* 2012). However in the present study, we did not simulate these differential accretion rates as specific to each fault strip, since there were different plant types and surface elevations in each fault strip. Rather used maximum observed accretion values from across our landscape, as dependent on elevation. Other factors exist which could affect future landscape change which have not been considered in this model, including land cover redistribution, barrier island migration, and overwash processes. Extreme storm forces are capable of affecting horizontal spatial pattern formation of land cover through

overwash processes (Feagin and Williams 2008). The spatial resolution of the DEM can also influence the spatial variability of topography derived from the DEM in low-relief systems, such as coastal dunes (Kim and Zheng 2001).

As corroborated by our findings, both eustatic- and faulting-induced changes can ultimately result in the destruction of vital wetland areas (White and Tremblay 1995, Feagin *et al.* 2005). From an ecological standpoint, RSLR can significantly alter the vegetation makeup of wetland communities (White and Morton 1997), can severely hamper the ability of wetlands to fulfill their natural functions, and can affect biodiversity (LaFever *et al.* 2007, Ross *et al.* 2009).

The findings in this study support the ability of simulation modeling techniques to project sea level rise and GIS data to predict RSLR and its impact on coastal regions (Yin *et al.* 2010); as the predictive modeling of the impacts of faulting in wetlands simulated land cover conversion as a function of fault-induced elevation change and compared the impact of specific rates of fault movement with predicted IPCC sea level rise projections. These findings further support the ability of GIS modeling to quantify the amount of expected change in wetlands and the potential impacts of climate change on coastal ecosystems (Costanza *et al.* 1990, Titus and Richman 2001) through the use of LiDAR and DEMs (Hennecke and Cowell 2000, LaFever *et al.* 2007, Snow and Snow 2009, Feagin *et al.* 2010) at a landscape scale.

4. SUMMARY AND CONCLUSIONS

This study presents evidence of significant changes in wetland land cover classes over time. The results demonstrate the different effects of RSLR through the changes and transitions between land cover classes in contrasting situations. Further examination of these shifts in land cover classes proximal to the fault scarp demonstrated the relationship between distance from the fault and faulting activity.

Faulting and RSLR affect vertical accretion and sedimentation. Rapid water level rise can force wetland land cover class conversion regardless of whether this relative rise is caused by vertical fault displacement or eustatic sea level rise, resulting in the destruction of vital wetland areas. Through the monitoring of coastal faulting, this research presents a threshold relative rise rate where the elevation change rate exceeds the wetlands ability to compensate for the change occurring. Current recorded conditions of sea level rise along the Texas Gulf Coast exceed this threshold value and leave a grim outlook for regions similar to this study area. Coastal faulting activity provided a key point of reference to understanding and evaluating the potential impacts of climate-induced RSLR on wetland ecosystems.

Though the use and employment of remote sensing, change detection, and GIS, sea level rise, RSLR, and their impacts on coastal wetland ecosystems, were monitored, evaluated, visualized, and quantified, further supporting the ability of these tools to provide useful information to ecosystem managers to mitigate change.

Wetland land cover classification is often a challenge and the use of historical imagery can present further challenges in regards to classification methods, further compounding the complex nature of land cover classification in wetlands. Preprocessing techniques can be useful and are valuable when using automated classification methods. Despite technology advancements, manual image interpretation can often still be a valuable tool; however, methods exist which can ease the intensity. For example, object oriented approaches can prove useful through the segmentation of an image into homogenous segments, followed by the export of the segmentation polygons to a GIS to then be manually classified by an analyst.

Further development in this field will further improve wetland vegetation classification performance. Due to the inherent value that wetlands contribute to coastal ecosystems, and the extensive technology now available, further inquiry into the application of remote sensing techniques with respect to wetland classification would provide significant benefit to researchers across a broad range of disciplines.

REFERENCES

Baker, C., Lawrence, R., Montagne, C., and Patten, D., 2006. Mapping wetlands and riparian areas using Landsat ETM+ imagery and decision-tree-based models. *Wetlands,* 26 (2), 465-474.

Chan, A.W., and Zoback, M.D., 2007. The role of hydrocarbon production on land subsidence and fault reactivation in the Louisiana coastal zone. *Journal of Coastal Research*, 23 (3), 771-786.

Craft, C., Clough, J., Ehman, J., Joye, S., Park, R., *et al.*, 2009. Forecasting the effects of accelerated sea level rise on tidal marsh ecosystems services. *Frontiers in Ecology and Environment*, 7, 73-78.

Cline, M., Feagin, R.A., Yeager, K.M., & Van Alstyne, J.M., 2011.Fault-induced wetland loss at Matagorda, Texas, USA: Land cover changes from 1943 to 2008. *Geocarto International,* 26, 633-645.

Costanza, R., Sklar, F.H., and White, M.L., 1990. Modeling coastal landscape dynamics. *BioScience,* 40, 91-107.

Day, J.W., Pont, D., Hensel, P.E., and Ibanez, C., 1995. Impacts of sea level rise on deltas in the Gulf of Mexico and the Mediterranean: The importance of pulsing events to sustainability. *Estuaries and Coasts*, 18 (4), 636-647.

Diegel, F.A. , Karlo, J.F., Schuster, D.C., and Shoup, R.C., 1995. Cenozoic structural evolution and tectono-stratigraphic framework in the northern Gulf Coast continental margin. In: Jackson, M. P. A. , D. G. Roberts , S. Snelson. *Salt*

Tectonics: A Global Perspective, AAPG Memoir, volume 65. Tulsa, Oklahoma AAPG. 109–151.

Dokka, R.K. , Sella, G.F., and Dixon, T.H., 2006. Tectonic control of subsidence and southward displacement of southeast Louisiana with respect to stable North America. *Geophysical Research Letters,* 33, L23308, 1-5.

Feagin, R.A., Yeager, K.M., Brunner, C.A., and Paine, J.G. 2012. Active fault motion in a coastal wetland: Matagorda Peninsula, Texas. *Geomorphology*, In Press.

Feagin, R.A., Gonzalez, G., Martínez, M.L., and Costanza, R., 2010a. Salt marsh zonal migration and ecosystem service change in response to global sea level rise: A case study from an urban region. *Ecology and Society*, 15 (4), 1-15.

Feagin, R.A., Yeager, K.M., Brunner, C.A., and Paine, J., 2010b. Vegetation transition and sedimentary responses to fault-induced sea level rise. A Report to NICCR-DOE. NICCR Coastal Center, Tulane University, New Orleans, LA.

Feagin, R. A., and Williams, A.M., 2008. Sediment spatial patterns in a Hurricane Katrina overwash fan on Dauphin Island, Alabama, U.S.A. *Journal of Coastal Research*, 24 (4), 1063-1070.

Feagin, R.A., Sherman, D.J., and Grant, W.E., 2005. Coastal erosion, global sea level rise, and the loss of sand dune plant habitats. *Frontiers in Ecology and Environment*, 3, 359-364.

Halabisky, M., Moskal, L.M., and Hall, S.A., 2011. Object-based classification of semi-arid wetlands. *Journal of Applied Remote Sensing,* 5, 1-13.

Hartig, E.K., Gornitz, V., Kolker, A., Mushacke, F., and Fallon, D., 2002. Anthropogenic and climate-change impacts on salt marshes of Jamaica Bay, New York City. *Wetlands*, 22, 71-89.

Hennecke, W.G., and Cowell, P.J. 2000. GIS modeling of impacts of an accelerated rate of sea level rise on coastal inlets and deeply embayed shorelines. *Environmental Geosciences,* 7(3), 137-148.

Intergovernmental Panel on Climate Change (IPCC), 2007. Meehl, G. A., Stocker, T. F., Collins, W. D., Friedlingstein, P., Gaye, A.T., *et al.* Global climate projections. *In:* Solomon S., Qin D., Manning M., Chen, Z. Marquis, K.B., *et al.* (Eds). *Climate Change 2007: The Physical Science Basis*. Contribution of Working Group I to the Fourth Assessment Report of the Intergovernmental Panel on Climate Change. Cambridge, UK: Cambridge University Press.

Irons, J.R. and Petersen, G.W., 1981. Texture transforms of remote sensing data. *Remote Sensing of Environment,* 11, 359-370.

Jallow, B.P., Barrow, M.K.A., and Leatherman, S.P., 1996. Vulnerability of the coastal zone of the Gambia to sea level rise and development of response strategies and adaptation options. *Climate Research*, 6 (2), 165-177.

Keddy, P.A., Fraser, L.H., Solomeshch, A.I., Junk, W.J., Campbell, D.R., *et al.*, 2009. Wet and wonderful: The world's largest wetlands are conservation priorities. *BioScience*, 59 (1), 39-54.

Kim, D., Yu, K.B., and Park, S.J., 2008. Identification and visualization of complex spatial pattern of coastal dune soil properties ssing GIS-based terrain analysis and geostatistics. *Journal of Coastal Research*, 24 (4C), 50-60.

Kim, D., and Zheng, Y., 2001. Scale-dependent predictability of DEM-based landform attributes for soil spatial variability in a coastal dune system. *Geoderma*, 164, 181-194.

Kreitler, C.W., 1976. Lineations and faults in the Texas coastal zone. Report of Investigations No. 85. Bureau of Economic Geology, University of Texas, Austin, TX.

LaFever, D.H., Lopez, R.R., Feagin, R.A., and Silvy, N.J., 2007. Predicting the impacts of future sea level rise on an endangered Lagomorph. *Environmental Management*, 40, 430-437.

Leatherman, S.P., 2001. Social and economic costs of sea level rise. *International Geophysics*, 75, 181-223.

Lee, J.K., Park, R.A., and Mausel, P.W., 1992. Application of geoprocessing and simulation modeling to estimate impacts of sea level rise on the Northeast Coast of Florida. *Photogrammetric Engineering and Remote Sensing*, 58, 1579-1586.

Mallman, E.P. and Zoback, M.D., 2007. Subsidence in the Louisiana coastal zone due to hydrocarbon production. *Journal of Coastal Research,* 5, 443-449.

McFadden, L., Nicholls, R.J., Vafeidis, A., and Tol, R.S.J., 2007. A methodology for modeling coastal space for global assessment. *Journal of Coastal Research,* 23(4), 911-920.

Menon, S., Sorberon, J., Li, X., and Peterson, A.T., 2010. Preliminary global assessment of terrestrial biodiversity consequences of sea level rise mediated by climate change. *Biodiversity and Conservation*, 19, 1599-1609.

Mitsch, W.J. and Gosslink, J.G., 2000a. The value of wetlands: importance of scale and landscape setting. *Ecological Economics*, 35, 25-33.

Mitsch, W.J. and Gosslink, J.G., 2000b. *Wetlands* (3rd ed.). New York: John Wiley & Sons.

Moorhead, K.K. and Brinson, M.M., 1995. Response of wetlands to rising sea level in the lower coastal plain of North Carolina. *Ecological Society of America*, 5, 261-271.

Morton, R.A. and Bernier, J.C., 2010. Recent subsidence-rate reductions in the Mississippi Delta and their geological implications. *Journal of Coastal Research*, 26, 555-561.

Morton, R.A., Bernier, J.C., and Barras, J.A., 2006. Evidence of regional subsidence and associated interior wetland loss induced by hydrocarbon production, Gulf Coast region, USA. *Environmental Geology*, 50, 261-274.

Morton, R.A., Paine, J.G., and Blum, M.D., 2000. Responses of stable bay-margin and barrier-island systems to Holocene sea level highstands, Western Gulf of Mexico. *Journal of Sedimentary Research*, 70, 478-490.

Ozesmi, S.L. and Bauer, M.E., 2002. Satellite remote sensing of wetlands. *Wetlands Ecology and Management*, 10, 381-402.

Rahmstorf, S., 2007. A semi-empirical approach to projecting future sea level rise. *Science*, 315, 368-370.

Railroad Commission of Texas, 2011. "Oil, Gas, and Pipeline Data" [map]. *Public GIS Map Viewer* [computer files], Austin, TX.

Reyes, E., Georgiou, I., Reed, D., and McCorquodale, A., 2005. Using models to evaluate the effects of barrier islands on estuarine hydrodynamics and habitats: A numerical experiment. *Journal of Coastal Research*, SI (44), 176 – 185.

Richardson, C., 1994. Ecological functions and human values in wetlands: A framework for assessing forestry impacts. *Wetlands*, 14, 1-9.

Ross, M.S., O'Brien, J.J., Ford, R.G., Zhang, K., and Morkill, A., 2009. Disturbance and the rising tide: The challenge of biodiversity management on low-island ecosystems. *Frontiers in Ecology and Environment*, 7, 471-478.

Salvador, A., 1987. Late Triassic-Jurassic paleogeography and origin of Gulf of Mexico basin. *American Association of Petroleum Geologists Bulletin*, 71, 419–451.

Shirley, L.J., and Battaglia, L.L., 2008. Projecting fine resolution land-cover dynamics for a rapidly changing terrestrial-aquatic transition in Terrebonne Basin, Louisiana, U.S.A. *Journal of Coastal Research*, 24(6), 1545-1554.

Snow, M.M., and Snow, R.K. 2009. Modeling, monitoring, and mitigating sea level rise. *Management of Environmental Quality*, 20(4), 422-433.

Thieler, E.R., and Hammar-Klose, E.S., 2000. National assessment of coastal vulnerability to future sea level rise: preliminary results for the US Gulf of Mexico coast. *USGS Open-File Report*, 00-179.

Titus, J.G. and Richman, C., 2001. Maps of lands vulnerable to sea level rise: Modeled elevations along the US Atlantic and Gulf coasts. *Climate Research*, 18, 205-228.

Twilley, R.R., and Rivera-Monroy, V.H., 2005. Developing performance measures of mangrove lands using simulation models of hydrology, nutrient, biochemistry, and community dynamics. *Journal of Coastal Research*, SI (40), 79-93.

White, W.A. and Morton, R.A., 1997. Wetland losses related to fault movement and hydrocarbon production, southeastern Texas coast. *Journal of Coastal Research*, 13, 1305-1320.

White, W.A. and Tremblay, T.A., 1995. Submergence of wetlands as a result of human-induced subsidence and faulting along the upper Texas Gulf Coast. *Journal of Coastal Research*, 11, 788-807.

Yin, J., Griffies, S.M., and Stouffer, R.J., 2010. Spatial variability of sea level rise in twenty-first century projections. *Journal of Climate*, 23, 4585-4607.

Zhang, Y., Lu, D., Yang, B., Sun, C., and Sun, M., 2011. Coastal wetland vegetation classification with a Landsat Thematic Mapper image. *International Journal of Remote Sensing*, 32 (2), 545-561.

VITA

Marie Denise Cline
(281) 723-7013
marie.cline@tamu.edu
1500 Research Plaza, Office 215, MS 2120, College Station, Texas 77845

PUBLICATIONS:

Cline, M.D., Feagin, R.A., Yeager, K.M., & Van Alstyne, J.M. 2011. Fault-induced wetland loss at Matagorda, Texas, USA: land cover changes from 1943 to 2008. *Geocarto International,* 26 (8), 633-645.

Locke, S.L., **Cline, M.D.**, et al. 2005. From the Field: A web-based digital camera for monitoring remote wildlife. *Wildlife Society Bulletin,* 33 (2), 761-765.

EDUCATION:

Texas A&M University, College Station, TX
M.S. in Rangeland Ecology and Management, August 2010 – August 2012
Graduate Certificate in Remote Sensing
Research interests: Remote Sensing, GIS, and Spatial Analysis

Texas A&M University, College Station, TX
B.S. in Wildlife and Fisheries Sciences, December 16, 2006
Option: Conservation Biology and Biodiversity
Minor: Rangeland Ecology and Management